



# Factors That Control the Formation of Dendrites and Other Morphologies on Lithium Metal Anodes

Louise Frenck<sup>1,2†</sup>, Gurmukh K. Sethi<sup>2,3†</sup>, Jacqueline A. Maslyn<sup>1,2†</sup> and Nitash P. Balsara<sup>1,2,4\*\*</sup>

<sup>1</sup> Department of Chemical and Biomolecular Engineering, University of California, Berkeley, Berkeley, CA, United States,

<sup>2</sup> Lawrence Berkeley National Laboratory, Materials Science Division, Berkeley, CA, United States, <sup>3</sup> Department of Materials Science and Engineering, University of California, Berkeley, Berkeley, CA, United States, <sup>4</sup> Lawrence Berkeley National Laboratory, Joint Center for Energy Storage Research (JCESR), Berkeley, CA, United States

## OPEN ACCESS

### Edited by:

Claire Villevieille,  
Université Grenoble Alpes, France

### Reviewed by:

Federico Bella,  
Politecnico di Torino, Italy  
Michel Bernard Armand,  
CIC Energigune, Spain

### \*Correspondence:

Nitash P. Balsara  
nbalsara@berkeley.edu

### †ORCID:

Louise Frenck  
orcid.org/0000-0001-7116-2144

Gurmukh K. Sethi  
orcid.org/0000-0002-8966-385X

Jacqueline A. Maslyn  
orcid.org/0000-0002-6481-2070

Nitash P. Balsara  
orcid.org/0000-0002-0106-5565

### Specialty section:

This article was submitted to  
Electrochemical Energy Conversion  
and Storage,  
a section of the journal  
Frontiers in Energy Research

**Received:** 28 June 2019

**Accepted:** 04 October 2019

**Published:** 01 November 2019

### Citation:

Frenck L, Sethi GK, Maslyn JA and  
Balsara NP (2019) Factors That  
Control the Formation of Dendrites  
and Other Morphologies on Lithium  
Metal Anodes.  
Front. Energy Res. 7:115.  
doi: 10.3389/fenrg.2019.00115

Lithium metal is a promising anode material for next-generation rechargeable batteries, but non-uniform electrodeposition of lithium is a significant barrier. These non-uniform deposits are often referred to as lithium “dendrites,” although their morphologies can vary. We have surveyed the literature on lithium electrodeposition through three classes of electrolytes: liquids, polymers and inorganic solids. We find that the non-uniform deposits can be grouped into six classes: whiskers, moss, dendrites, globules, trees, and cracks. These deposits were obtained in a variety of cell geometries using both unidirectional deposition and cell cycling. The main result of the study is a figure where the morphology of electrodeposited lithium is plotted as a function of two variables: shear modulus of the electrolyte and current density normalized by the limiting current density. We show that specific morphologies are confined to contiguous regions on this two-dimensional plot.

**Keywords:** dendrite, lithium metal, electrolytes, limiting current, rechargeable batteries

## INTRODUCTION

There is growing interest in the nature of electrodeposition at lithium metal electrodes due to the current focus on increasing the energy density of rechargeable lithium batteries (Girishkumar et al., 2010; Balsara and Newman, 2013). However, many fundamental challenges must be addressed before lithium electrodes can be deployed in practical devices (Aurbach et al., 2000, 2002). One of the main challenges is the nucleation and growth of protrusions during battery charging (Selim and Bro, 1974; Besenhard and Eichinger, 1976; Epelboin, 2006), which limits the battery lifetime and compromises safety (Yamaki et al., 1998; Aurbach et al., 2002). These protrusions are often referred to as “lithium dendrites.” Strictly, the word “dendrite” implies a branched structure; we propose to not use this term as many non-dendritic morphologies have been reported in the literature.

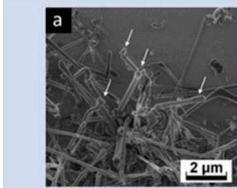
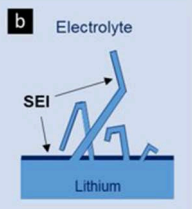
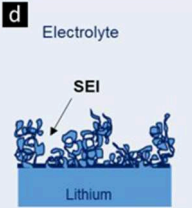
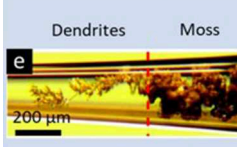
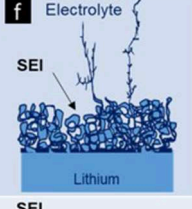
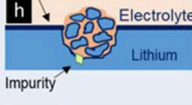
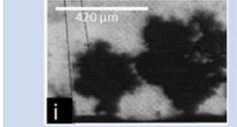
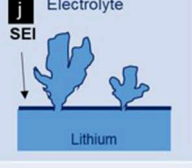
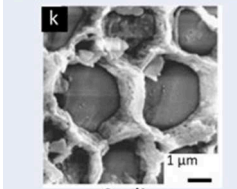
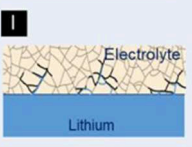
Lithium metal protrusions have been observed in electrodeposition and cycling experiments conducted in a wide array of electrolytes (Arakawa et al., 1993; Brissot et al., 1998; Ren et al., 2015). We focus on three classes of electrolytes: those based on organic liquids, organic polymers, and inorganic solids. The lithium ions are present in both liquid- and polymer-based electrolytes due to the addition of a suitable salt. In contrast, lithium ions are an integral part of the crystal structure of inorganic solid electrolytes. The passage of current results in salt concentration gradients in liquid- and polymer-based electrolytes (Chazalviel, 1990). On the other hand, these concentration gradients are absent when current flows through inorganic solid electrolytes. In principle, polymer

electrolytes can also be single ion conductors if the anion is covalently linked to the polymer chain (Bouchet et al., 2013). Compared to polymer electrolytes with added salt, there is little information about dendrite morphologies obtained in polymeric single-ion conductors (Cao et al., 2019; Dai et al., 2019). We have thus chosen to only discuss liquid and polymer electrolyte systems with added salt. Our objective is to identify the parameters that control the nature of lithium electrodeposition in liquid electrolytes, polymer electrolytes, and ceramic electrolytes.

The morphology of electrodeposited lithium is affected by many factors, such as current density, salt concentration where lithium is plating, tip radius of the protrusion, temperature, pressure (Yamaki et al., 1998; Gireaud et al., 2006) solid electrolyte interphase (SEI), and the ion transport and mechanical properties of electrolyte (Barton and Bockris, 1961; Diggle et al., 1969; Jana and García, 2017). While we have focused on the anode and the electrolyte, it is well-known that spontaneous reactions between lithium metal and all known electrolytes result in the formation of an SEI layer (Peled, 1979), which plays a central role in stable cycling (Tarascon and Armand, 2001; Meyerson et al., 2019). We have also glossed over the fact that liquid electrolytes are often contained within porous separators that are necessary for battery operation. The observed morphologies are grouped in six different classes described in **Table 1**. Important features of the lithium morphology are summarized in **Table 2**.

Whiskers emanating from the anode represent the simplest morphology of lithium protrusions. These are generally long and thin structures, with widths of about 1 μm and lengths ranging from 10 to 100 μm (see first entry in **Table 2**). Panel a in **Table 1** shows a scanning electron microscopy (SEM) image of whiskers. A schematic of whiskers is shown next to the SEM image in Panel b (**Table 1**). In this schematic, we represent the whiskers connected directly to the anode without an intervening SEI layer (Aurbach et al., 2002). We hypothesize that this must be the case; we are not aware of any direct support for our hypothesis. The whiskers are covered by an SEI layer (Peled, 1979; Aurbach et al., 1987) and surrounded by the electrolyte. Panel c in **Table 1** shows an SEM image of mossy lithium and a schematic of this morphology is shown in Panel d (**Table 1**). This electrodeposited lithium presents solid interconnected pebbles with electrolyte filling gaps and pores. Panels e,f in **Table 1** present lithium dendrites. Dendrites are thin-branched, fractal objects. Lithium globules are presented in Panels g,h (**Table 1**). These objects are found in confined regions, unlike whiskers, mosses and dendrites which tend to form across the entire electrode. Globules are nucleated at an impurity particle in the electrode. Panels i,j in **Table 1**, show lithium trees emanating from the electrode. Unlike mosses that are irregular in shape, the lateral size of trees increases with increasing distance from the electrode. Panels k,l

**TABLE 1** | Name, experimental visualization, and schematic of common morphologies of electrodeposited lithium. Images of whiskers, mosses, dendrites, globules, trees, and cracks are reproduced with permission from (a) Steiger et al. (2014), (b) Qian et al. (2015), (c) Bai et al. (2016), (d) Harry et al. (2015), (e) Brissot et al. (1998), and (f) Cheng et al. (2017).

Morphology	Image	Schematic
Whiskers		
Moss		
Dendrites		
Globules		
Trees		
Cracks		

in **Table 1** show lithium deposition through cracks in ceramic electrolytes. In this case, lithium protrusions grow through grain boundaries and result in cracking of the electrolyte. Typical sizes and aspect ratios of the protrusions described above are given in **Table 2**.

There have been many attempts to model the growth of metallic protrusions during electrodeposition from different electrolytes (Barton and Bockris, 1961; Diggle et al., 1969; Monroe and Newman, 2005; Voss and Tomkiewicz, 2006; Mayers et al., 2012). In the case of liquid- and polymer-based electrolytes,

**Abbreviations:** DEC, Diethyl carbonate; DMC, Dimethyl carbonate; EC, Ethylene carbonate; Li, Lithium metal electrode; LiClO<sub>4</sub>, Lithium perchlorate; LiF, Lithium fluoride; LiFSI, Lithium bis(fluorosulfonyl)imide; LiPF<sub>6</sub>, Lithium hexafluorophosphate; LiTFSI, Lithium bis (trifluoromethanesulfonyl) imide; LLZO, Li<sub>7</sub>La<sub>3</sub>Zr<sub>2</sub>O<sub>12</sub> ceramic electrolyte; PC, Propylene carbonate; PEO, Poly(ethylene oxide); SEI, Solid electrolyte interphase; SEM, Scanning electron microscopy; SEO, Poly(styrene) – b – poly(ethylene oxide); SiC, Silicon carbide.

**TABLE 2** | Name, description, characteristic width, and aspect ratio of electrodeposited lithium morphologies.

Name	Description	Width (μm)	Height (μm)	Aspect ratio (length/width)
Whiskers	Objects with minimal branching and kinks surrounded by excess electrolyte	0.1–5	10–100	100
Moss	Interconnected pebble-like objects with electrolyte within gaps and pores	10–50	–	1
Dendrites	Branched, fractal structures	1–20	100–600	10
Globules	Collections of compact globules nucleated on an impurity particle	20–150	20–150	1–2
Trees	Object with a narrow stem and a branched top	At the bottom 10–50 At the top 50–500	100–500	1–3
Cracks	Object growing through grain boundaries or structural weakness in the inorganic solid electrolyte	1	–	5

**TABLE 3** | The three categories of electrolytes covered in this review, with their description, order of magnitude of ionic conductivity,  $\kappa$ , order of magnitude of the salt diffusion coefficient,  $D$ , characteristic range of steady-state current fraction,  $\rho_+$ , and characteristic mechanical behavior at the temperature of interest.

Electrolyte	Description	Mechanical behavior	Order of magnitude of $\kappa$ [S.cm <sup>-1</sup> ]	Order of magnitude of $D$ [cm <sup>2</sup> .s <sup>-1</sup> ]	Order of magnitude of $\rho_+$
Liquid	Salt dissolved in traditional carbonate-based liquid electrolyte (e.g., EC, PC, DMC)	viscous	10 <sup>-2</sup>	10 <sup>-6</sup>	0.3–0.4
Polymer	Salt dissolved in a neutral polymer (e.g., PEO, SEO)	elastic	10 <sup>-4</sup> –10 <sup>-3</sup>	10 <sup>-8</sup> –10 <sup>-7</sup>	0.05–0.2
Inorganic solid	Solid ceramic with lithium ions in the lattice (e.g., LLZO)	solid	10 <sup>-4</sup>	–	1

the passage of current results in depletion of salt at the cathode where lithium is being deposited. The current density,  $i$ , at which the salt concentration at the cathode approaches zero is defined as the limiting current density,  $i_L$ . The depletion of salt has been implicated in lithium protrusion nucleation and growth (Chazalviel, 1990; Bai et al., 2016). However, lithium protrusions have been observed to nucleate and grow at current densities far below the limiting current (Rosso et al., 2001; Xu et al., 2014; Jana and García, 2017). The nucleation and growth of lithium protrusions is also affected by the modulus and other mechanical properties of the electrolyte (Monroe and Newman, 2003, 2005; Barai et al., 2017). The importance of limiting current has been recognized in the literature (Chazalviel, 1990; Bai et al., 2016; Barai et al., 2017; Maslyn et al., 2018).

In this review, we demonstrate that the lithium protrusion morphology obtained in different classes of electrolytes are mainly functions of two parameters: (1) current density normalized by the limiting current density and (2) modulus of the electrolyte. We present literature results for lithium protrusion morphology as a function of these two parameters on a “morphology diagram.” Each morphology is roughly restricted to contiguous regions on this diagram.

## METHODS

The classes of electrolytes covered in this review are given in **Table 3**. The first column in **Table 3** provides a description of these classes and gives typical examples. The second column describes the mechanical behavior of the electrolyte. The liquid and inorganic solid electrolytes are relatively simple from the mechanical point of view. Polymers on the other hand are

neither simple solids nor simple liquids. They exhibit both viscous and elastic properties depending on temperature and time-scale of observation. Additionally, **Table 3** includes the orders of magnitude of relevant electrochemical properties: conductivity,  $\kappa$ , salt diffusion coefficient,  $D$ , and steady-state current ratio,  $\rho_+$ . Conductivity is measured by ac impedance, salt diffusion coefficient is measured by restricted diffusion, and the steady-state current ratio is measured in lithium-lithium symmetric cells.

The steady-state current fraction deserves some clarification. This approach for characterization of electrolytes was pioneered by Bruce, Vincent, and Evans (Bruce and Vincent, 1987; Evans et al., 1987). In this approach, a fixed dc potential is applied to the symmetric cell and current is recorded as a function of time. At early times, the salt concentration in the electrolyte is uniform (as it is when the cell is at rest) and the current obtained under these circumstances is dictated by conductivity alone. We ignore contribution from interfacial impedance in this description; this is discussed extensively in the literature (Bruce and Vincent, 1987; Evans et al., 1987). We refer to the current obtained in the absence of concentration gradient as  $i_\Omega$ . The passage of time results in the establishment of salt concentration gradients, which, in turn, lead to a reduction of current. The ratio of the final steady-state current obtained in such an experiment,  $i_{SS}$  to  $i_\Omega$  is defined as the steady-state current fraction  $\rho_+$  (Gray and Bruce, 1995; Galluzzo et al., 2019). In the literature this fraction is often called the transference number,  $t_+$ . It is known however that  $\rho_+$  equals  $t_+$  for the case of dilute electrolytes that are thermodynamically ideal (i.e., when the salt activity coefficient is unity). Since practical electrolytes are never dilute, it is our understanding that the transference number is different from  $\rho_+$  in all of the electrolytes covered in this study. Nevertheless,

the steady-state current fraction is an important characteristic of electrolytes. The analysis presented in this paper makes extensive use of this characteristic.

## DISCUSSION

The systems chosen for this study are listed in **Table 4**. Each class of electrolytes is presented using a different color background: blue for liquid electrolytes listed first, red for polymer electrolytes listed second, and yellow for inorganic solid electrolytes listed third. The liquid electrolytes are alkyl-carbonate-based systems used in lithium-ion batteries. The alkyl carbonates of interest include ethylene carbonate (EC), dimethyl carbonate (DMC), diethylene carbonate (DEC), and propylene carbonate (PC). The salts dissolved in these liquids include bis (trifluoromethanesulfonyl)imide lithium salt (LiTFSI), lithium perchlorate (LiClO<sub>4</sub>), and lithium hexafluorophosphate (LiPF<sub>6</sub>). The second class is polymer electrolytes, which are composed of a neutral polymer, such as poly(ethylene oxide) (PEO) or block copolymer poly(styrene)-*b*-poly(ethylene oxide) (SEO). The salt dissolved in these polymers is usually LiTFSI or lithium bis(fluorosulfonyl)imide (LiFSI). The last class is inorganic solid electrolytes, which can be either classical crystalline solids with lithium ions in the lattice, such as Li<sub>7</sub>La<sub>3</sub>Zr<sub>2</sub>O<sub>12</sub> (LLZO) or glassy solids, such as 80Li<sub>2</sub>S-20P<sub>2</sub>S<sub>5</sub>.

The importance of limiting current has already been discussed above. However, this parameter is seldom measured directly by experiment. We thus use a simple expression for the limiting current taken from (Monroe and Newman, 2003),

$$i_L = \frac{2c_bDF}{(1 - \rho_+)L} \quad (1)$$

where  $c_b$  is the salt concentration in the conducting phase,  $F$  is the Faraday's constant, and  $L$  is the distance between the two electrodes. We have taken the liberty of replacing the transference number in equation (23.5) in Monroe and Newman (2003) by  $\rho_+$ . Equation 1 only applies to electrolytes containing added salt. It does not apply to single ion conductors.

In **Table 4**, we provide values for the parameters required to calculate  $i_L$ . For completeness we provide values for conductivity, though this parameter is not used in our analysis. The first entry in **Table 4** is the classical lithium-ion battery electrolyte. The formation of lithium protrusions in this electrolyte was studied using two different kind of cells: lithium-lithium symmetric cells and a half cell with carbon as the cathode. Protrusions were obtained after cycling the cells, indicated in the cycling/deposition column by 'C'. The electrochemical parameters were obtained from references (Valøen and Reimers, 2005; Dahbi et al., 2011) as indicated in the first entry in **Table 4**. In many of the entries in **Table 4**, electrochemical characterization data was obtained from different references, as is the case for the first entry. In such cases, the reference is provided below the parameter. In cases where electrochemical characterization data were presented along with lithium protrusion characterization, no references are provided

next to the characterization data. The parameter  $L$ , is the distance between the electrodes. In the case of composite cathodes like the carbon (graphite particles) used in the first entry, we ignore salt concentration gradients that occur within the electrolyte contained inside the pores of the composite cathode. In addition, when the cell has two different electrodes, one of the electrodes is always lithium metal and we are only concerned with electrodeposition of lithium on the lithium metal electrode. The second entry in **Table 4** is similar to the first entry except that the cell was not cycled. The formation of lithium protrusion was studied after one-directional electrodeposition, indicated in the cycling/deposition column by 'D'. In the third entry in **Table 4**, the copper cathode is electrochemically inactive. Lithium metal is deposited onto this cathode, which is similar to a lithium metal electrode after sufficient passage of current. Other entries related to liquid electrolytes in **Table 4** include surfaces treated with specific chemicals [e.g., copper treated with lithium fluoride (LiF) and lithium treated with silicon carbide (SiC)]. A majority of the liquid electrolytes studies reported in **Table 4** were conducted on lithium-lithium symmetric cells.

In many systems reported in **Table 4**, the parameters needed to estimate  $i_L$  were not reported in the lithium electrodeposition studies. We have relied on literature to estimate parameters in these cases. The deposition experiments for liquid electrolytes were conducted in the vicinity of room temperature (20°C to 30°C). We have not accounted for temperature variation between different studies. The values of  $i_L$  reported in **Table 4** vary from 0.06 to 380 mA.cm<sup>-2</sup>. While many parameters affect  $i_L$ , the wide range of  $i_L$  values are largely due to differences in  $L$  (see Equation 1). We posit that the differences in mechanical properties of liquid electrolytes are small, and therefore not relevant. We thus do not report the modulus of these systems in **Table 4**.

The work on lithium electrodeposition through polymers is restricted to PEO homopolymers and PEO containing block copolymers. The electrodeposition experiments are conducted at elevated temperatures (e.g., 90°C), due to poor ion transport in the vicinity of room temperature. The electrochemical parameters reported in **Table 4** are applicable at the temperature at which the electrodeposition was performed. In polymer electrolytes the values of  $i_L$  range from 0.001 to 4 mA.cm<sup>-2</sup>. The in-phase shear modulus,  $G'$ , of the polymers in the low frequency limit is also reported in **Table 4**. At the temperatures of interest, PEO homopolymers are rubbery liquids and in the low frequency limit  $G'$  is proportional to  $\omega^2$ , where  $\omega$  is the frequency. In other words, the shear modulus of PEO homopolymer is negligible at low frequencies. On the other hand, SEO block copolymers exhibit a frequency independent  $G'$  in the low frequency limit. This solid-like behavior is due to the presence of the glassy polystyrene domains. The values of  $G'$  reported for these systems is thus non-negligible.

The last set of entries in **Table 4** pertain to inorganic solid electrolytes. In these systems Li<sup>+</sup> is the only mobile ion and thus  $\rho_+ = 1$ . The limiting current in these systems cannot be calculated using Equation (1) (Monroe and Newman, 2003). The shear moduli of these materials are 4 orders of magnitudes larger than those of polymeric solids in **Table 4**.

**TABLE 4** | Properties of electrolytes and cells used to study lithium electrodeposition covered in this review.

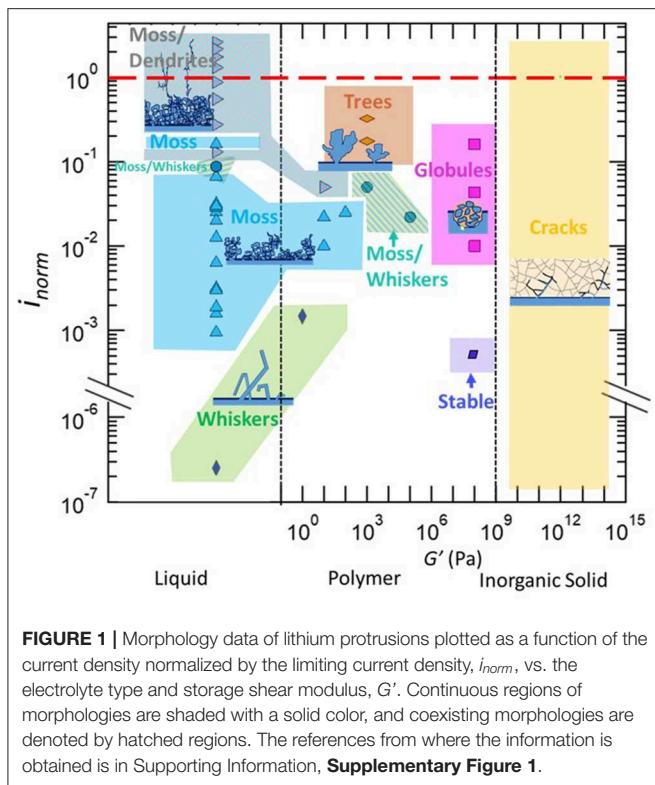
Electrolyte	G' (Pa)	$c_b$ (mol.L <sup>-1</sup> )	$\kappa$ (S.cm <sup>-1</sup> )	D (cm <sup>2</sup> .s <sup>-1</sup> )	$\rho^+$	L (cm)	i (mA.cm <sup>-2</sup> )	$i_L$ (mA.cm <sup>-2</sup> )	Type of cell used	Cycling/ Deposition	References
LiPF <sub>6</sub> EC:DMC ratio 1:1	–	1	1.0 × 10 <sup>-2</sup> Dahbi et al., 2011	2.5 × 10 <sup>-6</sup> Valøen and Reimers, 2005	0.39 Valøen and Reimers, 2005	0.1	1	8	Li/Li and Li/graphite	C	Kim and Yoon, 2004
LiPF <sub>6</sub> EC:DMC ratio 1:1	–	1	1.0 × 10 <sup>-2</sup> Dahbi et al., 2011	1.0 × 10 <sup>-6</sup>	0.38	0.03	1.09 to 50	20	Li/Li	D	Bai et al., 2016
LiPF <sub>6</sub> PC:DMC ratio 1:3	–	1	1.0 × 10 <sup>-2</sup> Dahbi et al., 2011	2.5 × 10 <sup>-6</sup> Valøen and Reimers, 2005	0.39 Valøen and Reimers, 2005	0.013	4	120	Li/Cu	D	Crowther and West, 2008
LiPF <sub>6</sub> EC:EMC ratio 3:7	–	1.2	1.0 × 10 <sup>-2</sup> Dahbi et al., 2011	2.5 × 10 <sup>-6</sup> Valøen and Reimers, 2005	0.39 Valøen and Reimers, 2005	0.0025	2	380	Li/Li <sub>4</sub> Ti <sub>5</sub> O <sub>12</sub>	C	López et al., 2009
LiClO <sub>4</sub> in PC	–	0.25	5.4 × 10 <sup>-3</sup> Werblan and Balkowska, 1993	2.2 × 10 <sup>-6</sup> Nishikawa et al., 2006	0.29 Mauro et al., 2005	0.0025	5	75	Li/Ni	D	Nishikawa et al., 2010
	–	1		1.3 × 10 <sup>-6</sup> Nishikawa et al., 2006			5	177			
LiPF <sub>6</sub> EC:DMC ratio 1:1	–	1	1.0 × 10 <sup>-2</sup> Dahbi et al., 2011	2.5 × 10 <sup>-6</sup> Valøen and Reimers, 2005	0.39 Valøen and Reimers, 2005	0.0025	0.5	316	Li/Cu and Li-LiF/Cu	D	Zhang et al., 2017
LiPF <sub>6</sub> EC:DMC ratio 1:1	–	1	1.0 × 10 <sup>-2</sup> Dahbi et al., 2011	2.5 × 10 <sup>-6</sup> Valøen and Reimers, 2005	0.39 Valøen and Reimers, 2005	0.0025	0.74 to 0.2	316	Li/Cu and Li/W	D	Steiger et al., 2014, 2015
LiPF <sub>6</sub> in EC:EMC	–	1	1.0 × 10 <sup>-2</sup> Dahbi et al., 2011	2.5 × 10 <sup>-6</sup> Valøen and Reimers, 2005	0.39 Valøen and Reimers, 2005	0.0025	0.3	316	Li/Li and Li/SiC	C	Sun et al., 2016
(LiPF <sub>6</sub> ), (LiTFSI), or LiFSI in DME, or DOL and PC	–	1	1.0 × 10 <sup>-2</sup> Dahbi et al., 2011	2.5 × 10 <sup>-6</sup> Valøen and Reimers, 2005	0.39 Valøen and Reimers, 2005	0.0025	0.2 to 8	316	Li/Li and Li/Cu	C	Qian et al., 2015
LiPF <sub>6</sub> in EC:DEC	–	1	1.0 × 10 <sup>-2</sup> Dahbi et al., 2011	2.5 × 10 <sup>-6</sup> Valøen and Reimers, 2005	0.39 Valøen and Reimers, 2005	0.0015	0.5	527	Li/Li and Li/graphene sheet	C	Bobnar et al., 2018
LiPF <sub>6</sub> EC:DMC ratio 1:1	–	1	1.0 × 10 <sup>-2</sup> Dahbi et al., 2011	2.5 × 10 <sup>-6</sup> Valøen and Reimers, 2005	0.39 Valøen and Reimers, 2005	0.0025	1	316	Li/Li	D	Zachman et al., 2018
LiPF <sub>6</sub> EC:DMC ratio 1:1	–	1	1.0 × 10 <sup>-2</sup> Dahbi et al., 2011	2.5 × 10 <sup>-6</sup> Valøen and Reimers, 2005	0.39 Valøen and Reimers, 2005	0.2	0.64	395	Li/Li	C	Eastwood et al., 2015
LiPF <sub>6</sub> or LiTFSI EC:DMC or EC:PC ratio 1:1	–	1	1.0 × 10 <sup>-2</sup> Dahbi et al., 2011	2.5 × 10 <sup>-6</sup> Valøen and Reimers, 2005	0.39 Valøen and Reimers, 2005	0.0695	1 to 50	11.4	Li/Li	D	Gireaud et al., 2006

(Continued)

TABLE 4 | Continued

Electrolyte	G' (Pa)	c <sub>b</sub> (mol.L <sup>-1</sup> )	κ (S.cm <sup>-1</sup> )	D (cm <sup>2</sup> .s <sup>-1</sup> )	ρ <sup>+</sup>	L (cm)	i (mA.cm <sup>-2</sup> )	i <sub>L</sub> (mA.cm <sup>-2</sup> )	Type of cell used	Cycling/Deposition	References
LITFSI and SEO (240–260)	10 <sup>8</sup> Harry et al., 2014	1.59	5.5 × 10 <sup>-4</sup> Villaluenga et al., 2018	4.70 × 10 <sup>-8</sup> Villaluenga et al., 2018	0.05 Pesko et al., 2018	0.003	0.175	4	Li/Li	C at 90°C	Harry et al., 2014, 2015, 2016; Schausser et al., 2014
LITFSI and PEO 30	10 <sup>9</sup> Stone et al., 2012	0.095	1.5 × 10 <sup>-3</sup> Pesko et al., 2018	3.5 × 10 <sup>-8</sup> Pesko et al., 2018	0.085 Pesko et al., 2018	0.2	0.1 to 0.5	0.0035	Li/Li and Li/Cu	C at 90°C	Dollé et al., 2002
LITFSI and PEO 300	10 <sup>8</sup> Stone et al., 2012	0.095	1.5 × 10 <sup>-3</sup> Pesko et al., 2018	6.00 × 10 <sup>-8</sup> Pesko et al., 2018	0.085 Pesko et al., 2018	0.0035	0.06	0.343	Li/Li	D at 90°C	Rosso et al., 2006
							0.01	0.06			
							0.1	0.06	0.0012		
LITFSI and PEO 30	10 <sup>9</sup> Stone et al., 2012	0.095	9.7 × 10 <sup>-4</sup> Pesko et al., 2018	3.5 × 10 <sup>-8</sup> Pesko et al., 2018	0.085 Pesko et al., 2018	0.2	0.2	4	Li/Li	C at 80°C	Brissot et al., 1998
LITFSI and PEO 60	10 <sup>9</sup> Stone et al., 2012	0.95	1.0 × 10 <sup>-5</sup> Pesko et al., 2018	6.00 × 10 <sup>-8</sup> Pesko et al., 2018	0.085 Pesko et al., 2018	0.02	0.05	0.6	Li/Li	D	Hirano, 2010
LITFSI and SEO (115–172)	10 <sup>8</sup> Harry et al., 2014	1.59	5.5 × 10 <sup>-4</sup> Pesko et al., 2018	7.37 × 10 <sup>-8</sup> Pesko et al., 2018	0.045 Pesko et al., 2018	0.004	0.02 to 0.64	4	Li/Li	D at 90°C	Maslyn et al., 2018
LITFSI and PEO 30	10 <sup>9</sup> Stone et al., 2012	0.095	9.1 × 10 <sup>-4</sup> Pesko et al., 2018	3.50 × 10 <sup>-8</sup> Pesko et al., 2018	0.085 Pesko et al., 2018	0.1	0.95	0.007	Li/Li	D at 80°C	Brissot et al., 1999, 2001
β-Li <sub>3</sub> PS <sub>4</sub>	10 <sup>12</sup> Baranowski et al., 2016	–	1.6 × 10 <sup>-4</sup> Liu et al., 2013	–	1	0.3	0.01 to 5	–	Li/Li	C/D	Porz et al., 2017; Seitzman et al., 2018
LLZO	5 × 10 <sup>10</sup>	–	2.0 × 10 <sup>-4</sup> Shao et al., 2016	–	1		0.015 to 0.50	–	Li/Li	C/D/C	Ren et al., 2015; Cheng et al., 2017; Porz et al., 2017)
80Li <sub>2</sub> S-20P <sub>2</sub> S <sub>5</sub>	2 × 10 <sup>10</sup> Kato et al., 2018	–	2.8 × 10 <sup>-4</sup> Sakuda et al., 2010	–	1		0.05 to 20	–	Li/Li	C	Nagao et al., 2013

We report shear modulus, G', the ionic conductivity, κ, diffusion coefficient, D, the current ratio, ρ<sub>+</sub> number or best estimated transference number, the applied current density, i, the measured or calculated limiting current, i<sub>L</sub>, the distance between the electrodes, L, the type of cell cycled, if the lithium was unidirectional electrodeposited (D) or cycled (C) and the reference. The number next to the polymer electrolytes refers to the number averaged molecular weight of the polymer in kg.mol<sup>-1</sup>.



There are many studies of lithium protrusion morphology in novel electrolytes such as ionic liquids and organic-inorganic composite electrolytes. We do not include them due to the unavailability of the necessary electrochemical characterization data.

Since theory suggests that the limiting current plays an important role (Chazalviel, 1990; Monroe and Newman, 2003; Bai et al., 2016; Barai et al., 2017; Maslyn et al., 2018), we define a normalized current density as the experimental current density over the limiting current density.

$$i_{norm} = \frac{i}{i_L} \tag{2}$$

Where  $i$  is the applied current density.

In **Figure 1**, we present results of lithium electrodeposition experiments that were listed in **Table 4**. The modulus of the electrolytes is given on the abscissa and the normalized current density is given on the ordinate. A red dashed line indicates where the applied current density to the cell equals the limiting current. All of the protrusion morphologies listed in **Table 1** occupy contiguous regions in **Figure 1** and are shaded in different colors with the corresponding cartoon for visual clarity. The vertical dashed lines in the figure distinguish the three different kinds of electrolytes considered in this review (**Table 3**):

(1) **Liquids.** In liquid electrolytes with negligible moduli, whiskers (green) are obtained in the regime  $i_{norm} = 10^{-7}$ . At this low normalized current density, the driving force for

lithium ion reduction is not sufficient to induce branching in the projecting structures. It is important to note that in this particular study, lithium electrodeposition was carried out without a separator. Increasing  $i_{norm}$  in liquid electrolytes results in the formation of mossy lithium (blue). This morphology is obtained in the range  $10^{-3} < i_{norm} < 7 \times 10^{-2}$ . In most studies mossy lithium was observed in coin cells where the electrolyte is contained in a porous separator. The spring in the coin cell does exert pressure on the cell components including the interface between lithium metal and the porous separator. It is possible that the mossy lithium seen at low values of  $i_{norm}$  are compacted whiskers due to the pressure exerted on them by the separator. Some evidence for this is presented below. Increasing  $i_{norm}$  to 0.08 results in coexistence of mossy and whiskers (hatched green and blue). Further increase of  $i_{norm}$  to 0.3 results in dendrites that grow on the top of the mossy deposit (hatched gray and blue). The cross-over from mossy to dendritic deposits occurs over a range of  $i_{norm}$  values, from 0.08 to 0.3. In this regime we see two isolated pockets: one where moss and whiskers coexist and one where only moss is observed (see **Figure 1**). There are no examples in **Table 4** where lithium dendrites are seen to grow directly from the planar anode.

(2) **Polymers.** Low modulus polymers ( $G' < 10$  Pa) exhibit behavior similar to liquids at low values of  $i_{norm}$ . At  $i_{norm} = 0.001$ , whiskers are seen in a cell that does not contain a separator. Note that at this value of  $i_{norm}$ , mossy lithium deposits have been observed in liquid cells with separator (see **Figure 1**). This suggests that some of the mossy deposits seen in liquid electrolytes may be due to the pressure exerted by the separator. Increasing  $i_{norm}$  to 0.01 results in the formation of moss, which is seen in the range between 0.01 and 0.04. At higher normalized current densities, coexisting moss/dendrites are seen. With higher modulus polymers ( $G' = 10^3$  Pa) and higher normalized current densities, coexisting moss/whiskers are seen for  $0.02 < i_{norm} < 0.05$ . At higher normalized current densities,  $i_{norm} \geq 0.2$  trees are observed (orange). Increasing the modulus of polymers to  $10^8$  Pa results in stable lithium deposition at  $i_{norm} = 0.005$ . While the current used under these conditions are too low for practical applications, it is important to note that whiskers are obtained at the same normalized current density in both liquids and polymers with  $G' < 10$  Pa. Increasing  $i_{norm}$  to 0.01 results in the formation of globular protrusions. This morphology is seen up to  $i_{norm} = 0.2$ .

(3) **Inorganic solids.** The three inorganic solid electrolytes in **Table 4** include crystal and glassy solids. In all cases failure due to the passage of current induces cracking (yellow) in the electrolyte. While lithium protrusions grow through grain boundaries in crystals, it is postulated that they grow through mechanically weak portions of glasses. In a recent study it was shown that grain boundaries in crystalline lithium ion conductors exhibit higher electronic conductivity than the bulk crystal (Han et al., 2019). This is one explanation for the observation of the growth of lithium protrusion in grain boundaries.

## CONCLUSION

We have surveyed the literature on electrodeposition of lithium through a variety of electrolytes: liquids, polymers, and inorganic solids. We have focused on the morphology of lithium protrusions that often emerged in these experiments. We show that these morphologies are governed by two parameters: shear modulus of the electrolyte and current density normalized by the limiting current density. The main result of this work is **Figure 1** where we plot the lithium protrusion morphology as a function of these two parameters. The different morphologies appear in contiguous regions in this figure, analogous to a phase diagram.

## AUTHOR CONTRIBUTIONS

LF, GS, and JM compiled information from the literature. LF, GS, JM, and NB wrote the manuscript.

## REFERENCES

- Arakawa, T., Tsukamoto, S., Nagamune Y., Nishioka, M., Lee, J.-H., and Arakawa, Y. (1993). Fabrication of InGaAs strained quantum wire structures using selective-area metal-organic chemical vapor deposition growth. *Jpn. J. Appl. Phys.* 32, 1377–1379. doi: 10.1143/JJAP.32.L1377
- Aurbach, D., Daroux, M. L., Faguy, P. W., and Yeager, E. (1987). Identification of surface films formed on lithium in propylene carbonate solutions. *J. Electrochem. Soc.* 134, 1611–1620. doi: 10.1149/1.2100722
- Aurbach, D., Zinigrad, E., Cohen, Y., and Teller, H. (2002). A short review of failure mechanisms of lithium metal and lithiated graphite anodes in liquid electrolyte solutions. *Solid State Ionics* 148, 405–416. doi: 10.1016/S0167-2738(02)00080-2
- Aurbach, D., Zinigrad, E., Teller, H., and Dan, P. (2000). Factors which limit the cycle life of rechargeable lithium (Metal) batteries. *J. Electrochem. Soc.* 147, 1274–1279. doi: 10.1149/1.1393349
- Bai, P., Li, J., Brushett, F. R., and Bazant, M. Z. (2016). Transition of lithium growth mechanisms in liquid electrolytes. *Energy Environ. Sci.* 9, 3221–3229. doi: 10.1039/C6EE01674J
- Balsara, N. P., and Newman, J. (2013). Comparing the energy content of batteries, fuels, and materials. *J. Chem. Educ.* 90, 446–452. doi: 10.1021/ed3004066
- Barai, P., Higa, K., and Srinivasan, V. (2017). Effect of initial state of lithium on the propensity for dendrite formation: a theoretical study. *J. Electrochem. Soc.* 164, A180–A189. doi: 10.1149/2.0661702jes
- Baranowski, L. L., Heveran, C. M., Ferguson, V. L., and Stoldt, C. R. (2016). Multi-scale mechanical behavior of the Li3PS4 solid-phase electrolyte. *ACS Appl. Mater. Interfaces* 8, 29573–29579. doi: 10.1021/acsami.6b06612
- Barton, J. L., and Bockris, J. O. (1961). The electrolytic growth of dendrites from ionic solutions. *Proc. R. Soc. Lond. A* 268, 485–505.
- Besenhard, J. O., and Eichinger, G. (1976). High energy density lithium cells. Part I. Electrolytes and anodes. *J. Electroanal. Chem.* 68, 1–18. doi: 10.1016/S0022-0728(76)80298-7
- Bobnar, J., Lozinšek, M., Kapun, G., Njel, C., Dedryvère, R., Genorio, B., et al. (2018). Fluorinated reduced graphene oxide as a protective layer on the metallic lithium for application in the high energy batteries. *Sci. Rep.* 8:5819. doi: 10.1038/s41598-018-23991-2
- Bouchet, R., Maria, S., Meziane, R., Aboulaich, A., Lienafa, L., Bonnet, J. P., et al. (2013). Single-ion BAB triblock copolymers as highly efficient electrolytes for lithium-metal batteries. *Nat. Mater.* 12, 452–457. doi: 10.1038/nmat3602
- Brissot, C., Rosso, M., Chazalviel, J.-N., Baudry, P., and Lascaud, S. (1998). *In situ* study of dendritic growth in lithium/PEO-salt/lithium cells. *Electrochim. Acta* 43, 1569–1574. doi: 10.1016/S0013-4686(97)10055-X
- Brissot, C., Rosso, M., Chazalviel, J.-N., and Lascaud, S. (1999). *In situ* concentration cartography in the neighborhood of dendrites growing in lithium/polymer-electrolyte/lithium cells. *J. Electrochem. Soc.* 146, 4393–4400. doi: 10.1149/1.1392649
- Brissot, C., Rosso, M., Chazalviel, J. N., and Lascaud, S. (2001). Concentration measurements in lithium/polymer-electrolyte/lithium cells during cycling. *J. Power Sources* 94, 212–218. doi: 10.1016/S0378-7753(00)00589-9
- Bruce, P. G., and Vincent, C. A. (1987). Steady state current flow in solid binary electrolyte cells. *J. Electroanal. Chem. Interfacial Electrochem.* 225, 1–17. doi: 10.1016/0022-0728(87)80001-3
- Cao, C., Li, Y., Feng, Y., Peng, C., Li, Z., and Feng, W. (2019). A solid-state single-ion polymer electrolyte with ultrahigh ionic conductivity for dendrite-free lithium metal batteries. *Energy Storage Mater.* 19, 401–407. doi: 10.1016/j.ensm.2019.03.004
- Chazalviel, J.-N. (1990). Electrochemical aspects of the generation of ramified metallic electrodeposits. *Phys. Rev. A* 42, 7355–7367. doi: 10.1103/PhysRevA.42.7355
- Cheng, E. J., Sharafi, A., and Sakamoto, J. (2017). Intergranular Li metal propagation through polycrystalline Li<sub>6</sub>.<sub>25</sub>Al<sub>0.25</sub>La<sub>3</sub>Zr<sub>2</sub>O<sub>12</sub> ceramic electrolyte. *Electrochim. Acta* 223, 85–91. doi: 10.1016/j.electacta.2016.12.018
- Crowther, O., and West, A. C. (2008). Effect of electrolyte composition on lithium dendrite growth. *J. Electrochem. Soc.* 155, A806–A811. doi: 10.1149/1.2969424
- Dabbi, M., Ghamouss, F., Tran-Van, F., Lemordant, D., and Anouti, M. (2011). Comparative study of EC/DMC LiTFSI and LiPF<sub>6</sub> electrolytes for electrochemical storage. *J. Power Sources* 196, 9743–9750. doi: 10.1016/j.jpowsour.2011.07.071
- Dai, K., Ma, C., Feng, Y., Zhou, L., Kuang, G., Zhang, Y., et al. (2019). A borate-rich, cross-linked gel polymer electrolyte with near-single ion conduction for lithium metal batteries. *J. Mater. Chem. A* 7, 18547–18557. doi: 10.1039/C9TA05938E
- Diggle, J. W., Despic, A. R., and Bockris, J. O. (1969). The mechanism of the dendritic electrocrystallization of zinc. *J. Electrochem. Soc.* 116, 1503. doi: 10.1149/1.2411588
- Dollé, M., Sannier, L., Beaudoin, B., Trentin, M., and Tarascon, J.-M. (2002). Live scanning electron microscope observations of dendritic growth in lithium/polymer cells. *Electrochem. Solid State Lett.* 5, A286–A289. doi: 10.1149/1.1519970
- Eastwood, D. S., Bayley, P. M., Chang, H. J., Taiwo, O. O., Vila-Comamala, J., Brett, D. J., et al. (2015). Three-dimensional characterization of electrodeposited lithium microstructures using synchrotron X-ray phase contrast imaging. *Chem. Commun.* 51, 266–268. doi: 10.1039/C4CC03187C
- Epelboin, I. (2006). Behavior of secondary lithium and aluminum-lithium electrodes in propylene carbonate. *J. Electrochem. Soc.* 127:2100. doi: 10.1149/1.2129354

## ACKNOWLEDGMENTS

Funding to support this work was provided by the Energy & Biosciences Institute through the EBI-Shell program. LF was supported by EBI-Shell. JM, GS, and NB were supported by the Assistant Secretary for Energy Efficiency and Renewable Energy, Office of Vehicle Technologies of the U.S. Department of Energy under Contract DE-AC02-05CH11231 under the Battery Materials Research Program. GS and JM also acknowledge funding from a National Science Foundation Graduate Student Research Fellowship (2016218210 and DGE 2752814, respectively).

## SUPPLEMENTARY MATERIAL

The Supplementary Material for this article can be found online at: <https://www.frontiersin.org/articles/10.3389/fenrg.2019.00115/full#supplementary-material>

- Evans, J., Vincent, C. A., and Bruce, P. G. (1987). Electrochemical measurement of transference numbers in polymer electrolytes. *Polymer* 28, 2324–2328. doi: 10.1016/0032-3861(87)90394-6
- Galluzzo, M. D., Maslyn, J. A., Shah, D. B., and Balsara, N. P. (2019). Ohm's law for ion conduction in lithium and beyond-lithium battery electrolytes. *J. Chem. Phys.* 151:020901. doi: 10.1063/1.5109684
- Gireaud, L., Grugeon, S., Laruelle, S., Yrieix, B., and Tarascon, J.-M. (2006). Lithium metal stripping/plating mechanisms studies: a metallurgical approach. *Electrochem. Commun.* 8, 1639–1649. doi: 10.1016/j.elecom.2006.07.037
- Girishkumar, G., McCloskey, B., Luntz, A. C., Swanson, S., and Wilcke, W. (2010). Lithium–air battery: promise and challenges. *J. Phys. Chem. Lett.* 1, 2193–2203. doi: 10.1021/jz1005384
- Gray, F. M., and Bruce, P. G. (1995). *Solid State Electrochemistry*, ed. P. G. Bruce. Cambridge: Cambridge University Press, 157–158.
- Han, F., Westover A. S., Yue, J., Fan, X., Wang, F., Chi, M., et al. (2019). High electronic conductivity as the origin of lithium dendrite formation within solid electrolytes. *Nat. Energy* 4, 187–196. doi: 10.1038/s41560-018-0312-z
- Harry, K. J., Hallinan, D. T., Parkinson, D. Y., MacDowell, A. A., and Balsara, N. P. (2014). Detection of subsurface structures underneath dendrites formed on cycled lithium metal electrodes. *Nat. Mater.* 13, 69–73. doi: 10.1038/nmat3793
- Harry, K. J., Higa, K., Srinivasan, V., and Balsara, N. P. (2016). Influence of electrolyte modulus on the local current density at a dendrite tip on a lithium metal electrode. *J. Electrochem. Soc.* 163, A2216–A2224. doi: 10.1149/2.0191610jes
- Harry, K. J., Liao, X., Parkinson, D. Y., Minor, A. M., and Balsara, N. P. (2015). Electrochemical deposition and stripping behavior of lithium metal across a rigid block copolymer electrolyte membrane. *J. Electrochem. Soc.* 162, A2699–A2706. doi: 10.1149/2.0321514jes
- Jana, A., and Garcia, R. E. (2017). Lithium dendrite growth mechanisms in liquid electrolytes. *Nano Energy* 41, 552–565. doi: 10.1016/j.nanoen.2017.08.056
- Kato, A., Yamamoto, M., Sakuda, A., Hayashi, A., and Tatsumisago, M. (2018). Mechanical properties of Li<sub>2</sub>S-P<sub>2</sub>S<sub>5</sub> glasses with lithium halides and application in all-solid-state batteries. *ACS Appl. Energy Mater.* 1, 1002–1007. doi: 10.1021/acsaem.7b00140
- Kim, W. S., and Yoon, W. Y. (2004). Observation of dendritic growth on Li powder anode using optical cell. *Electrochim. Acta* 50, 541–545. doi: 10.1016/j.electacta.2004.03.066
- Liu, S., Imanishi, N., Zhang, T., Hirano, A., Takeda, Y., Yamamoto, O. et al. (2010). Lithium dendrite formation in Li/poly(ethylene oxide)–lithium Bis(trifluoromethanesulfonyl)imide and N-Methyl-N-propylpiperidinium Bis(trifluoromethanesulfonyl)imide/Li Cells. *J. Electrochem. Soc.* 157, A1092–A1098. doi: 10.1149/1.3473790
- Liu, Z., Fu, W., Payzant, E. A., Yu, X., Wu, Z., Dudney, N. J., et al. (2013). Anomalous high ionic conductivity of nanoporous  $\beta$ -Li<sub>3</sub>PS<sub>4</sub>. *J. Am. Chem. Soc.* 135, 975–978. doi: 10.1021/ja3110895
- López, C. M., Vaughey, J. T., and Dees, D. W. (2009). Morphological transitions on lithium metal anodes. *J. Electrochem. Soc.* 156, A726–A729. doi: 10.1149/1.3158548
- Maslyn, J. A., Loo, W. S., McEntush, K. D., Oh, H. J., Harry, K. J., Parkison, D. Y., et al. (2018). Growth of lithium dendrites and globules through a solid block copolymer electrolyte as a function of current density. *J. Phys. Chem. C* 122:acs.jpcc.8b06355. doi: 10.1021/acs.jpcc.8b06355
- Mauro, V., D'Aprano, A., Croce, F., and Salomon, M. (2005). Direct determination of transference numbers of LiClO<sub>4</sub> solutions in propylene carbonate and acetonitrile. *J. Power Sources* 141, 167–170. doi: 10.1016/j.jpowsour.2004.09.015
- Mayers, M. Z., Kaminski, J. W., and Miller, T. F. (2012). Suppression of dendrite formation via pulse charging in rechargeable lithium metal batteries. *J. Phys. Chem. C* 116, 26214–26221. doi: 10.1021/jp309321w
- Meyerson, M. L., Sheavly, J. K., Dolocan, A., Greffin, M. P., Pandit, A. H., Rodriguez, R., et al. (2019). The effect of local lithium surface chemistry and topography on solid electrolyte interphase composition and dendrite nucleation. *J. Mater. Chem. A* 7, 14882–14894. doi: 10.1039/C9TA03371H
- Monroe, C., and Newman, J. (2003). Dendrite growth in lithium/polymer systems. *J. Electrochem. Soc.* 150, A1377–A1384. doi: 10.1149/1.1606686
- Monroe, C., and Newman, J. (2005). The impact of elastic deformation on deposition kinetics at lithium/polymer interfaces. *J. Electrochem. Soc.* 152, A396–A404. doi: 10.1149/1.1850854
- Nagao, M., Hayashi, A., Tatsumisago, M., Kanetsuku, T., Tsuda, T., and Kuwabata, S. (2013). *In situ* SEM study of a lithium deposition and dissolution mechanism in a bulk-type solid-state cell with a Li<sub>2</sub>S–P<sub>2</sub>S<sub>5</sub> solid electrolyte. *Phys. Chem. Chem. Phys.* 15, 18600–18606. doi: 10.1039/c3cp51059j
- Nishikawa, K., Fukunaka, Y., Sakka, T., Ogata, Y. H., and Selman, J. R. (2006). Measurement of LiClO<sub>4</sub>[sub 4] diffusion coefficient in propylene carbonate by Moiré pattern. *J. Electrochem. Soc.* 153, A830–A834. doi: 10.1149/1.2178648
- Nishikawa, K., Mori, T., Nishida T., Fukunaka, Y., Rosso, M., and Homma, T. (2010). *In situ* observation of dendrite growth of electrodeposited Li metal. *J. Electrochem. Soc.* 157, A1212–A1217. doi: 10.1149/1.3486468
- Peled, E. (1979). The electrochemical behavior of alkali and alkaline earth metals in nonaqueous battery systems—the solid electrolyte interphase model. *J. Electrochem. Soc.* 126:2047. doi: 10.1149/1.2128859
- Pesko, D. M., Sawhney, S., Newman, J., and Balsara, N. P. (2018). Comparing two electrochemical approaches for measuring transference numbers in concentrated electrolytes. *J. Electrochem. Soc.* 165, A3014–A3021. doi: 10.1149/2.0231813jes
- Porz, L., Swamy, T., Sheldon, B. W., and Rettenwander, D. (2017). Mechanism of lithium metal penetration through inorganic solid electrolytes. *Adv. Energy Mater.* 166, A984–A995. doi: 10.1002/aenm.201701003
- Qian, J., Henderson, W. A., Xu, W., Bhattacharya, P., Engelhard, M., Borodin, O., et al. (2015). High rate and stable cycling of lithium metal anode. *Nat. Commun.* 6:6362. doi: 10.1038/ncomms7362
- Ren, Y., Shen, Y., Lin, Y., and Nan, C. W. (2015). Direct observation of lithium dendrites inside garnet-type lithium-ion solid electrolyte. *Electrochem. Commun.* 57, 27–30. doi: 10.1016/j.elecom.2015.05.001
- Rosso, M., Brissot, C., Teyssot, A., Dolle, M., Sannier, L., Tarscon, J. M., et al. (2006). Dendrite short-circuit and fuse effect on Li/polymer/Li cells. *Electrochim. Acta* 51, 5334–5340. doi: 10.1016/j.electacta.2006.02.004
- Rosso, M., Gobron, T., Brissot, C., Chazalviel, J., and Lascaud, S. (2001). Onset of dendritic growth in lithium / polymer cells. *J. Power Sources* 98, 804–806. doi: 10.1016/S0378-7753(01)00734-0
- Sakuda, A., Hayashi, A., Hama, S., and Tatsumisago, M. (2010). Preparation of highly lithium-ion conductive 80Li<sub>2</sub>S·20P<sub>2</sub>S<sub>5</sub> thin-film electrolytes using pulsed laser deposition. *J. Am. Ceramic Soc.* 93, 765–768. doi: 10.1111/j.1551-2916.2009.03442.x
- Schauser, N. S., Harry, K. J., Parkinson, D. Y., Watanabe, H., and Balsara, N. P. (2014). Lithium dendrite growth in glassy and rubbery nanostructured block copolymer electrolytes. *J. Electrochem. Soc.* 162, A398–A405. doi: 10.1149/2.0511503jes
- Seitzman, N., Guthrey, H., Sulas, D. B., Platt, H. A. S., Ai-Jassim, M., Pylypenko, S. (2018). Toward all-solid-state lithium batteries: three-dimensional visualization of lithium migration in  $\beta$ -Li<sub>3</sub>PS<sub>4</sub> ceramic electrolyte. *J. Electrochem. Soc.* 165, A3732–A3737. doi: 10.1149/2.0301816jes
- Selim, R., and Bro, P. (1974). Some observations on rechargeable lithium electrodes in a propylene carbonate electrolyte. *J. Electrochem. Soc.* 121:1457. doi: 10.1149/1.2401708
- Shao, C., Liu, H., Yu, Z., Zheng, Z., Sun, N., and Diao, C. (2016). Structure and ionic conductivity of cubic Li<sub>7</sub>La<sub>3</sub>Zr<sub>2</sub>O<sub>12</sub> solid electrolyte prepared by chemical co-precipitation method. *Solid State Ionics* 287, 13–16. doi: 10.1016/j.ssi.2016.01.042
- Steiger, J., Kramer, D., and Mönig, R. (2014). Mechanisms of dendritic growth investigated by *in situ* light microscopy during electrodeposition and dissolution of lithium. *J. Power Sources* 261, 112–119. doi: 10.1016/j.jpowsour.2014.03.029
- Steiger, J., Richter, G., Wenk, M., Kramer, D., and Mönig, R. (2015). Comparison of the growth of lithium filaments and dendrites under different conditions. *Electrochem. Commun.* 50, 11–14. doi: 10.1016/j.elecom.2014.11.002
- Stone, G. M., Mullin, S. A., Teran, A. A., Hallinan, D. T. Jr., Minor, A. M., Hexemer, A., et al. (2012). Resolution of the modulus versus adhesion dilemma in solid polymer electrolytes for rechargeable lithium metal batteries. *J. Electrochem. Soc.* 159, A222–A227. doi: 10.1149/2.030203jes
- Sun, F., Zielke, L., Markötter, H., Hilger, A., Zhou, D., Moroni, R., et al. (2016). Morphological evolution of electrochemically plated/stripped lithium microstructures investigated by synchrotron X-ray phase contrast tomography. *ACS Nano* 10, 7990–7997. doi: 10.1021/acsnano.6b03939

- Tarascon, J.-M., and Armand, M. (2001). Issues and challenges facing rechargeable lithium batteries. *Nature* 414, 359–367. doi: 10.1038/35104644
- Valøen, L. O., and Reimers, J. N. (2005). Transport properties of LiPF<sub>6</sub>-based Li-ion battery electrolytes. *J. Electrochem. Soc.* 152, A882–A891. doi: 10.1149/1.1872737
- Villaluenga, I., Pesko, D. M., Timachova, K., Feng, Z., Newman, J., Srinivasan, V., et al. (2018). Negative Stefan-Maxwell diffusion coefficients and complete electrochemical transport characterization of homopolymer and block copolymer electrolytes. *J. Electrochem. Soc.* 165, A2766–A2773. doi: 10.1149/2.0641811jes
- Voss, R., and Tomkiewicz, M. (2006). Computer simulation of dendritic electrodeposition. *J. Electrochem. Soc.* 132, 371–375. doi: 10.1149/1.2113841
- Werblan, L., and Białkowska, A. (1993). Concentrated electrolyte solutions in organic solvents. Their specific conductance and analysis of Casteel–Amis equation. *J. Electroanal. Chem.* 354, 25–38. doi: 10.1016/0022-0728(93)80321-8
- Xu, W., Wang, J., Ding, F., Chen, X., Nasybulin, E., Zhang, Y., et al. (2014). Lithium metal anodes for rechargeable batteries. *Energy Environ. Sci.* 7, 513–537. doi: 10.1039/C3EE40795K
- Yamaki, J. I., Tobishima, S. I., Hayashi, K., Saito, K., Nemoto, Y., and Arakawa, M. (1998). A consideration of the morphology of electrochemically deposited lithium in an organic electrolyte. *J. Power Sources* 74, 219–227. doi: 10.1016/S0378-7753(98)00067-6
- Zachman, M. J., Tu, Z., Choudhury, S., Archer, L. A., and Kourkoutis, L. F. (2018). Cryo-STEM mapping of solid–liquid interfaces and dendrites in lithium-metal batteries. *Nature* 560, 345–349. doi: 10.1038/s41586-018-0397-3
- Zhang, X. Q., Chen, X., Xu, R., Cheng, X. B., Peng, H. J., Zhang, R., et al. (2017). Columnar lithium metal anodes. *Angew. Chemie Int. Ed.* 56, 14207–14211. doi: 10.1002/anie.201707093

**Conflict of Interest:** The authors declare that the research was conducted in the absence of any commercial or financial relationships that could be construed as a potential conflict of interest.

Copyright © 2019 Frenck, Sethi, Maslyn and Balsara. This is an open-access article distributed under the terms of the Creative Commons Attribution License (CC BY). The use, distribution or reproduction in other forums is permitted, provided the original author(s) and the copyright owner(s) are credited and that the original publication in this journal is cited, in accordance with accepted academic practice. No use, distribution or reproduction is permitted which does not comply with these terms.

## SYMBOLS

- $c_b$  – Salt concentration ( $\text{mol.L}^{-1}$ )  
 $D$  – Salt diffusion coefficient ( $\text{cm}^2.\text{s}^{-1}$ )  
 $F$  – Faraday constant ( $96485 \text{ C.mol}^{-1}$ )  
 $\kappa$  – Ionic conductivity ( $\text{S.cm}^{-1}$ )  
 $\omega$  – Frequency ( $\text{rad.s}^{-1}$ )  
 $G'$  – Shear modulus  
 $\rho_+$  – Steady-state current fraction  
 $i$  – Applied current density ( $\text{mA.cm}^{-2}$ )  
 $i_L$  – Limiting current density ( $\text{mA.cm}^{-2}$ )  
 $i_{\Omega}$  – Current obtained in the absence of salt concentration gradient (A)  
 $i_{norm}$  – Normalized current density  
 $i_{SS}$  – Steady-state current (A)  
 $L$  – Distance between the electrodes (cm)  
 $t_+$  – Transference number.